Received: 30 April 2020 | Revised: 22 June 2020 | Accepted: 11 July 2020

DOI: 10.1002/ardp.202000137

FULL PAPER

DPhG ARCH PHARM Archiv der Pharmazie

New nanodrug design for cancer therapy: Its synthesis, formulation, in vitro and in silico evaluations

Yasemin Budama-Kilinc[1] | Serda Kecel-Gunduz[2] | Burak Ozdemir[1] | Bilge Bicak[2] | Gizem Akman[3] | Busra Arvas[4] | Feray Aydogan[4] | Cigdem Yolacan[4]

[1]Department of Bioengineering, Yildiz Technical University, Davutpasa Campus, Istanbul, Turkey

[2]Department of Physics, Science Faculty, Istanbul University, Istanbul, Turkey

[3]Department of Biology, Science Faculty, Istanbul University, Istanbul, Turkey

[4]Department of Chemistry, Yildiz Technical University, Davutpasa Campus, Istanbul, Turkey

Correspondence
Cigdem Yolacan, Department of Chemistry, Yildiz Technical University, Davutpasa Campus, 34010 Esenler, Istanbul, Turkey.
Email: cigdemyolacan@hotmail.com

Funding information
TUBITAK, Grant/Award Numbers: 115S132, 117S097; Yildiz Technical University, Grant/Award Number: FBA-2017-3168

Abstract

The aim of this study was to develop a novel nanosize drug candidate for cancer therapy. For this purpose, (*S*)-methyl 2-[(7-hydroxy-2-oxo-4-phenyl-2*H*-chromen-8-yl)methyleneamino]-3-(1*H*-indol-3-yl)propanoate (ND3) was synthesized by the condensation reaction of 8-formyl-7-hydroxy-4-phenylcoumarin with L-tryptophan methyl ester. Its controlled release formulation was prepared and characterized by different spectroscopic and imaging methods. The cytotoxic effects of ND3 and its controlled release formulation were evaluated against MCF-7 and A549 cancer cell lines, and it was found that both of them have a toxic effect on cancer cells. For drug design and process development, the molecular docking analysis technique helps to clarify the effects of some DNA-targeted anticancer drugs to determine the interaction mechanisms of these drugs on DNA in a shorter time and at a lower cost. By using the molecular docking analysis and DNA binding assays, the interaction between the synthesized compound and DNA was elucidated and non-binding interactions were also determined. To predict the pharmacokinetics, and thereby accelerate drug discovery, the absorption, distribution, metabolism, excretion and toxicity values of the synthesized compound were determined by in silico methods.

KEYWORDS

anticancer, coumarin derivative, DNA binding, molecular docking, nanoparticle

1 | INTRODUCTION

Cancer is a common fatal disease caused by the uncontrolled growth of cells that have been altered by some effects. It is an important health problem that is considered the second most common cause of death after cardiovascular diseases all over the world. Surgery, chemotherapy and radiotherapy are the main therapeutic approaches to systematic cancer treatment. However, the treatment outcome with these methods is generally poor. Thus, it is very important to find an effective alternative treatment for cancer.[1] Various chemotherapeutic drugs for cancer treatment have been developed, but these drugs severely affect healthy tissues such as the hematopoietic system, bone marrow, gastrointestinal epithelial cells and hair follicles. Multidrug resistance (MDR) is another important difficulty in cancer treatment. Due to the side effects and MDR of the current chemotherapeutic agents,[2] the development of effective anticancer drugs with promising bioactivity and important therapeutic effects[3] and limited toxicity[4] is still a great struggle and urgent need for medicinal chemists.

Chemotherapeutic drugs are systemically active and cannot target cancer cells. High dosage of chemotherapeutic drugs causes severe side effects like the destruction of bone marrow cells, which impairs the erythrocytes' production, cardiotoxicity, nephrotoxicity, hepatotoxicity and hematotoxicity. To overcome these problems, nanoparticles (NPs) are used in cancer treatment. NPs provide several advantages in cancer diagnosis and treatment by targeting antigens or biomarkers that are specific to cancer cells.[5–8] An NP-mediated drug delivery system can eliminate drug or drug carrier side effects

significantly. In addition, the design of NPs may result in increased drug effectiveness at lower doses and reduce multiple drug resistance effects. The major advantage of nanotechnology is targeted drug delivery to the site of the disease.[9] Encapsulation of drugs in NPs has gained great attention as an important approach to the controlled delivery of the active drug to the target organs. The size, encapsulation efficiency and release kinetics are important features of these carrier NPs. The biocompatibility of these systems is another important factor to allow their use. If the interaction of the material with the body without any induction of toxicity and immunogenic, thrombogenic and carcinogenic responses occurs, it has high biocompatibility and can be used safely as a drug delivery system.[10] Polycaprolactone (PCL) is one of the certain polymers of the American Food and Drug Administration that have been approved for drug use. The hydrophobic structure of micro- and nanosized particles produced with PCL prevents the drug or active substances from dissolving and dispersing in body fluids. It is frequently used in tissue engineering applications, in particular, and drug production.[11] In addition, as the drug is loaded, nanosized PCL spheres follow selective targeting; they carry drugs to only the diseased region in the body.[12]

Coumarins that contain benzopyran-2-one ring system are an important class of heterocyclic compounds. Natural and synthetic coumarins have crucial pharmaceutical properties such as anticancer, antiviral, antibacterial, antifungal, antioxidant and anti-inflammatory effects.[13–18] Coumarin derivatives can be synthesized and functionalized to add desired properties by easy synthetic procedures. Due to their potential applications in cancer therapy, many studies have been reported on the design and synthesis of coumarin derivatives to improve their anticancer potential and investigation of their anticancer effects on various human tumor cell lines.[19–22] There are also some papers on the activity mechanism of coumarin derivatives on cancer cells.[23] The design and synthesis of new coumarin derivatives with a promising effect on cancer cells has been attracting the researchers, due to the encouraging improvements in the activity. Coumarins have low biodistribution due to their low solubility in the aqueous solution. Nowadays, nanoformulations are used to overcome solubility limitations.

For the synthesis of new drugs with improved selective activity and more clinical effectiveness, determining the interaction between synthesized molecules and DNA is crucial for rational drug design. Plant-derived polyphenolic compounds such as coumarin have a large number of biological and pharmacological properties. To reveal the interaction between the newly synthesized compound, which is coumarin derivative, and DNA, the DNA binding mode has been indicated by using various experimental and theoretical techniques such as DNA binding assays and molecular docking analysis. Ultraviolet (UV)–visible (Vis) absorbance spectra and molecular docking analysis show the interaction between the synthesized compound and DNA. The ADME (absorption, distribution, metabolism, excretion) calculations allow to understand and predict the pharmacokinetic properties of the synthesized compound with its molecular structure and properties using computer modeling.[24–26] ADME properties, which are essential to ensure drug-like pharmacokinetic profiles of the synthesized compound, were also calculated using Molinspiration, SwissADME and PreADMET servers.

2 | RESULTS AND DISCUSSION

In this study, (*S*)-methyl 2-[(7-hydroxy-2-oxo-4-phenyl-2*H*-chromen-8-yl)methyleneamino]-3-(1*H*-indol-3-yl)propanoate (ND3) was prepared by the condensation reaction of 8-formyl-7-hydroxy-4-phenylcoumarin (**2**) with L-tryptophan methyl ester (Scheme 1). The structure of the compound was determined by its spectral data, and it was concluded that they are in accordance with the structure. Then, its DNA-binding activity was investigated via experimental and theoretical methods.

2.1 | HOMO–LUMO and UV–Vis analysis results

HOMO and LUMO are molecular orbital types that give the ionization potential and the electron affinity of the molecule, which are called "highest occupied molecular orbital" and "lowest unoccupied

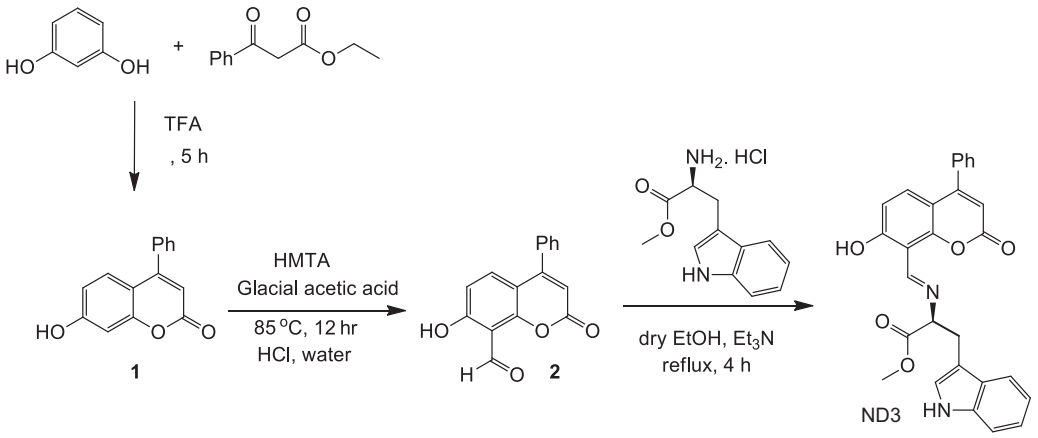

SCHEME 1 The synthesis of ND3

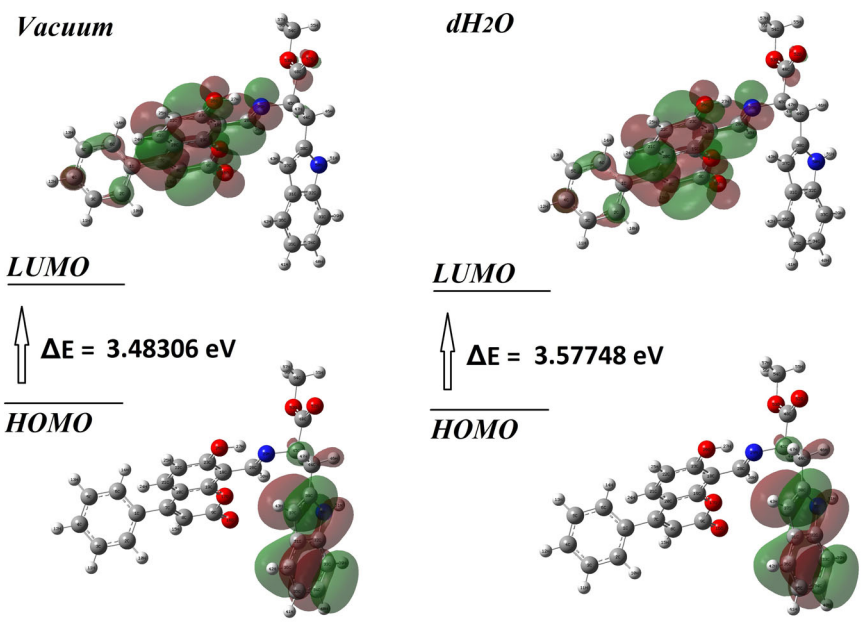

FIGURE 1 The energy gap and the highest occupied molecular orbital (HOMO) and lowest unoccupied molecular orbital (LUMO) energies of ND3

molecular orbital," respectively. The energy difference between the HOMO and the LUMO, which is an important indicator of stability and also reflects the chemical activity, generally corresponds to the lowest energy electronic excitation possible in a molecule. Molecules with a small HOMO–LUMO energy gap are defined as soft molecules, whereas larger ones are defined as hard molecules.[24,25] The energy gap and HOMO and LUMO energies were determined using TD-DFT/B3LYP 6-311++G(d,p), and the pictorial illustrations of the frontier molecular orbitals are shown in Figure 1 and tabulated in Tables 1 and 2. The HOMO was located over the indol ring and LUMO was presented over iminocoumarin ring, and the HOMO--LUMO transition stands for an electron density transfer from indolylethyl group to the iminocoumarin ring with 3.48 and 3.57 eV, for vacuum and dH_2O medium, respectively. The synthesized compound with a small HOMO–LUMO energy gap has soft molecule properties with high chemical reactivity, low kinetic stability and high polarization ability. The ionization potential $I(-EHOMO) = 5.74$ and 5.90 eV, electron affinity $A(-ELUMO) = 2.26$ and 2.32 eV, the electronegativity $\chi = (I + A)/2 = 4$ and 4.11 eV, chemical potential $\mu = -(I + A)/2 = -4$ and −4.11 eV, and hardness $\eta = (I - A)/2 = 1.74$ and 1.78 eV values were also calculated for the synthesized compound, as shown in Table 2 for vacuum and dH_2O medium, respectively. Absorption wavelength λ (nm) and excitation energies E (eV) of ND3 obtained computationally in the dH_2O solution and vacuum medium are tabulated in Table 3.

For the design of new anticancer drugs, DNA binding assay is a useful method to understand the mechanism of drug interaction with DNA.[27,28] UV–Vis spectroscopy is the most common instrumental method for DNA binding assay. This method is based on monitoring the change of absorption spectra of the drug in increasing concentrations of DNA, and the noncovalent interactions between the drug and DNA take place in three different ways: electrostatic, intercalation and groove binding.[28,29]

Figure 2 presents the obtained absorption spectra of ND3 with the addition of the different CT-DNA concentrations, and a change in absorbance intensity with hypochromism at 295 and 356 nm was determined. It was observed that the 14% hypochromism and 5-nm bathochromic shift (red shift) occurred at 295 nm, and 15% hypochromism and 4-nm bathochromic shift (red shift) occurred at 356 nm.

The hypochromic effect and red shift are observed as a result of binding of drug active substances to DNA by intercalation.[27,30]

TABLE 1 Calculated molecular orbital energies (eV) and energy differences of ND3

TD-B3LYP/6-311++G(d,p)							
	E_{LUMO+1}	E_{LUMO}	E_{HOMO}	E_{HOMO-1}	$\Delta E_{HOMO-LUMO}$	$\Delta E_{(HOMO)-(LUMO+1)}$	$\Delta E_{(HOMO-1)-(LUMO)}$
Vacuum	−2.00	−2.26	−5.74	−6.17	3.48	3.73	3.90
dH_2O	−2.02	−2.32	−5.90	−6.34	3.57	3.87	4.02

Abbreviations: HOMO, highest occupied molecular orbital; LUMO, lowest unoccupied molecular orbital.

TABLE 2 The calculated values of ionization potential, electron affinity, electronegativity, and chemical hardness for the ND3 molecule

Vacuum	TD-DFT/6-311++G(d,p)	Energy (AU)	Energy (eV)
Vacuum			
HOMO energy	E_{HOMO}	−0.21116	−5.74596
LUMO energy	E_{LUMO}	−0.08316	−2.26290
Ionization potential	$I = -E_{HOMO}$	0.21116	5.74596
Electron affinity	$A = -E_{LUMO}$	0.08316	2.26290
Electronegativity	$\chi = (I + A)/2$	0.14716	4.00443
Chemical potential	$\mu = -(I + A)/2$	−0.14716	−4.00443
Chemical hardness	$\eta = (I - A)/2$	0.064	1.74153
ΔE (gap)	$E_{LUMO} - E_{HOMO}$	0.128	3.48306
dH_2O			
HOMO energy	E_{HOMO}	−0.21685	−5.90079
LUMO energy	E_{LUMO}	−0.08538	−2.32331
Ionization potential	$I = -E_{HOMO}$	0.21685	5.90079
Electron affinity	$A = -E_{LUMO}$	0.08538	2.32331
Electronegativity	$\chi = (I + A)/2$	0.151115	4.11205
Chemical potential	$\mu = -(I + A)/2$	−0.151115	−4.11205
Chemical hardness	$\eta = (I - A)/2$	0.065735	1.78874
ΔE (gap)	$E_{LUMO} - E_{HOMO}$	0.13147	3.57748

Abbreviations: HUMO, highest occupied molecular orbital; LUMO, lowest unoccupied molecular orbital; TD-DFT, time-dependent density functional theory.

The red shift of the absorption spectrum indicates that the difference of the HOMO and LUMO energy levels decreases, and the drug molecule interacts with DNA.[31] The drug molecules, intercalating and/or groove binding with DNA, are important anticancer and antimicrobial agents for clinical applications.[32] In this study, after considering the results of DNA binding assay and in silico calculations, the anticancer efficiency of ND3 was investigated using in vitro cell culture against two different cancer cell lines.

In vitro cell culture studies were performed against MCF-7 and A549 cell lines, and 3-(4,5-dimethylthiazol-2-yl)-2,5-diphenyltetrazolium bromide (MTT) assay was used to evaluate the cytotoxicity of ND3. As seen in Figure 3, ND3 increased the cytotoxicity in dose-dependent manner on both cell lines as compared with control groups ($p < .05$). The average IC_{50} values were determined as 41 μg/ml (88 μM) for the A549 cell line and 72 μg/ml (155 μM) for MCF-7 cell line, according to MTT assay.

Considering the in vitro cell results, ND3's nanoformulation was produced to provide slow and controlled release in the cancer area. Bioavailability of ND3 was aimed to increase by preparing of nano-formulation.

ND3-loaded PCL NPs were prepared following the double-emulsion technique. The desired drug concentration can be maintained for a long time by encapsulation of drugs, and therefore the encapsulation efficiency and loading capacity are important terms in nanoformulation production.[33] The standard curve of ND3 (Figure 4) was used to determine the encapsulation efficiency and loading capacity. The encapsulation efficiency was calculated as 93% by using Equation 1. Loading capacity was calculated as 13.8% using

TABLE 3 Calculated absorption wavelengths λ (nm), excitation energies E (eV) and oscillator strengths (f) of ND3 along with transition levels and assignments in dH_2O and vacuum medium

TD-B3LYP/6-311++G(d,p)						
	E (eV)	λ (nm)	f	Major contributors	Symmetry	
dH_2O	3.1204	397.33	0.0017	H→L	91%	Singlet-A
	3.3835	366.44	0.0021	H→L+1	90%	Singlet-A
	3.6078	343.66	0.0067	H−1→L	95%	Singlet-A
Vacuum	3.0100	411.91	0.0017	H→L	88%	Singlet-A
				H→L+1	11%	
	3.2698	379.18	0.0012	H→L	11%	Singlet-A
				H→L+1	88%	
	3.4810	356.17	0.0055	H−1→L	94%	Singlet-A

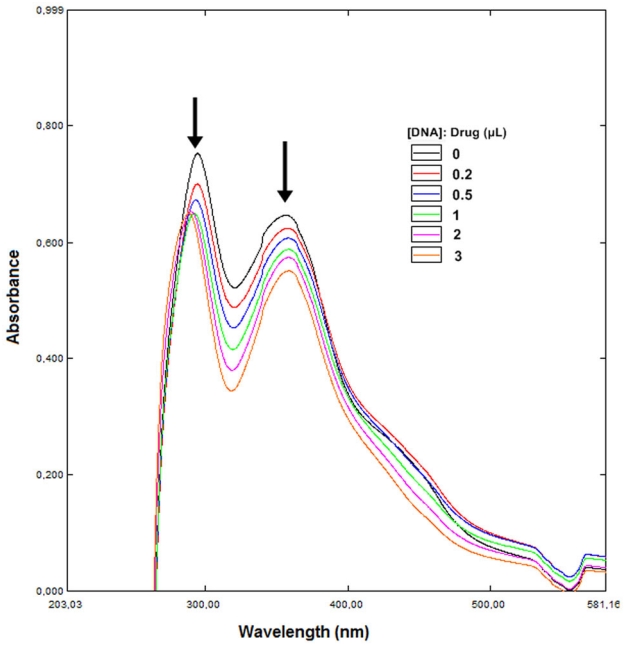

FIGURE 2 Absorption spectra of the compound in the absence and presence of increasing amounts of calf thymus DNA at room temperature in Tris-HCl/NaCl buffer (pH 7.2)

Equation 2 by comparing the total amount of encapsulated ND3 in the synthesized NPs to the total amount of NPs. This means that each 1 mg ND3-loaded PCL NPs contained 0.138 mg ND3:

$$H(\%) = \frac{A_i - A_S}{A_i} \times 100, \quad (1)$$

where A_i is the absorbance intensity of the substance in free form and A_s is the absorbance intensity of the substance after the addition of DNA at maximum concentration:

$$\text{Viability } \% = \frac{\text{Absorbance of experimental group}}{\text{Absorbance of control group}} \times 100. \quad (2)$$

The physicochemical properties such as average particle size, polydispersity index and ζ potential are crucial parameters for nano-formulated drugs, as they affect the drug distribution, cellular uptake, and toxicity. In this study, the average particle size, polydispersity index (PdI) and ζ potential values of NPs were determined with dynamic light scattering (DLS) technique. The results of free PCL NPs are given in Figure 5, and it was observed that the average particle size and ζ potential value were 206.9 nm and −7.62 mV, respectively. As seen from the figure, free PCL NPs had a narrow size distribution with 0.043 of the PdI value.

The DLS results of ND3-loaded PCL NPs are given in Figure 6. The average particle size and ζ potential values were 279.4 nm and −3.41 mV, respectively. It was found that ND3-loaded PCL NPs also had a narrow size distribution with 0.210 of the PdI value.

The in vitro ND3 release from PCL NPs was studied at predetermined time intervals in a phosphate-buffered solution (PBS) at pH 7.2 to simulate the physiological pH. It was found that ND3 release within the first 24 hr was 44.56% of the actual loading, corresponding to 49.9 µg ND3/mg PCL. It was seen from Figure 7, the release study was completed within 144 hr and 96.6% of the ND3 was released.

The Ames test is one of the short-time test systems, and it is a reliable assay that gives precise results about the mutagenicity of chemical substances. In this study, the mutagenicity of ND3 on *Salmonella typhymurium* TA100 and TA98 strains was determined with Ames/*Salmonella* Mutagenicity Assay. According to the results of the in vitro release study of ND3, five different concentrations of ND3 (112, 108, 90, 78 and 72 µg/plate) were used in the experiment. The number of colonies of application concentrations and the number of colonies of the negative control group were compared to evaluate the results. The sample, which doubled the number of colonies observed in the negative control, was evaluated as mutagenic.[34] The data obtained from the experimental and control groups were compared using the SPSS program, and $p < .05$ was accepted as significant in all statistical evaluations. As seen from Table 4 and Figure 8, it was found that none of the concentrations

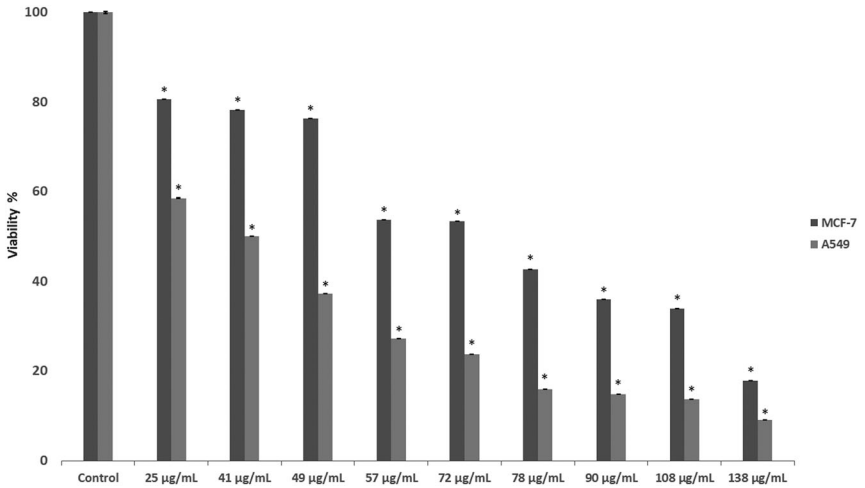

FIGURE 3 Cell viability results of ND3 on MCF-7 and A549 cell lines

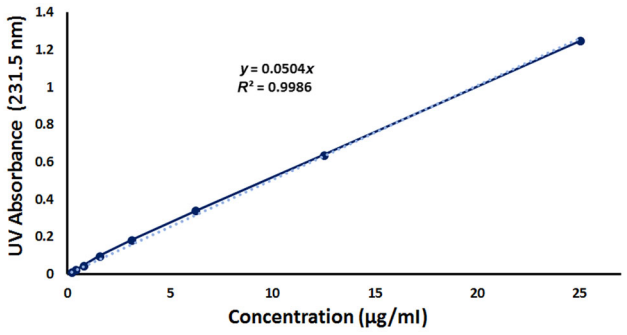

FIGURE 4 The standard curve of ND3

evaluated caused the basepair change or frameshift mutation and DNA damage ($p < .05$).

The surface morphology of the ND3-loaded PCL NPs was determined by SEM. As shown in Figure 9 with different magnification, SEM images indicated that ND3-loaded PCL NPs were spherical in shape, with a uniform distribution, and they had nonaggregated morphology.

The cytotoxic effect of ND3-loaded PCL NPs is shown in Figure 10. All concentrations have a toxic effect on both cell lines as compared with the control group ($p < .05$). In addition to this, it was also determined that ND3-loaded PCL NP was more effective than ND3 on A549 cells at 25, 41 and 49 µg/ml concentrations and 41 µg/ml on MCF-7 cells ($p < .05$).

2.2 | Molecular docking analysis results

The molecular docking analysis revealed that the synthesized compound binds with the B-DNA dodecamer in nine different conformations, and the most stable binding pose is at −8.8 kcal/mol energy with the largest negative binding energy (Table 5 and Figure 11). The close interactions between DNA and the synthesized compound were formed with deoxy guanosine (DG10, DG12, DG14 and DG16) and deoxy adenosine (DA17 and DA18), deoxy cytosine (DC9 and DC11), and deoxy thymine (DT19) base, and they are shown in Figure 11. As clearly seen from Figure 12, the synthesized compound was preferentially attached to the DNA. In total, the oxygen atom of the synthesized ligand formed a stable binding pose by forming 4 hydrogen bonds with the guanine (DG10, DG16) residues of DNA. Hydrogen bonds play a very considerable role in the interaction of the synthesized ligand with DNA, as more hydrogen bonding interactions (Table 5b) provide a stronger binding at higher stability and produce lower negative binding energy (−8.8 kcal/mol). The O1 atom of ligand and DG10 (H3 and H22 atoms) and DG16 (H21 and H22 atoms) of A and B chain of B-DNA dodecamer formed hydrogen bonds with 2.5, 3.1, 2.4 and 3.0 Å bond lengths, respectively. The root mean squared deviation (RMSD) values of synthesized compounds bound by B-DNA dodecamer are also tabulated in Table 6. The DNA binding activity of the synthesized compound was evaluated through DNA binding assays and molecular docking analysis method.

2.3 | ADME analysis results

To estimate the pharmacokinetic parameters of the synthesized compound to be a drug candidate, the ADME profile was calculated using in silico method, and absorption (A), distribution (D), metabolism (M) and excretion (E) values are given in Tables S1 and S2. The octanol–water partition coefficient, logP, which defines molecular hydrophobicity, affects drug absorption, bioavailability, hydrophobic drug–receptor interactions, metabolism and toxicity of molecules. The molecular polar surface area[35] is defined as the sum of the surfaces of polar atoms (usually oxygen, nitrogen, and bound hydrogen atoms) in a molecule; this value correlates very well with human intestinal absorption, the permeability of the Caco-2 monolayers, and blood–brain barrier penetration. Molecular volume is another feature that is related to the transport properties of molecules, such as intestinal absorption or blood–brain barrier

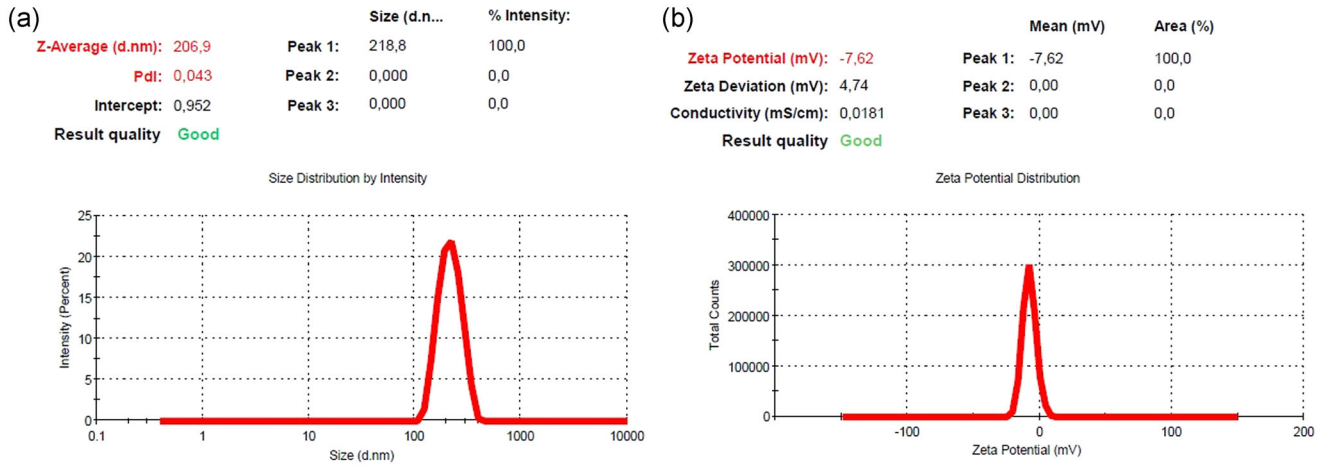

FIGURE 5 Dynamic light scattering results of free polycaprolactone nanoparticles: (a) average particle size and (b) ζ potential graphics

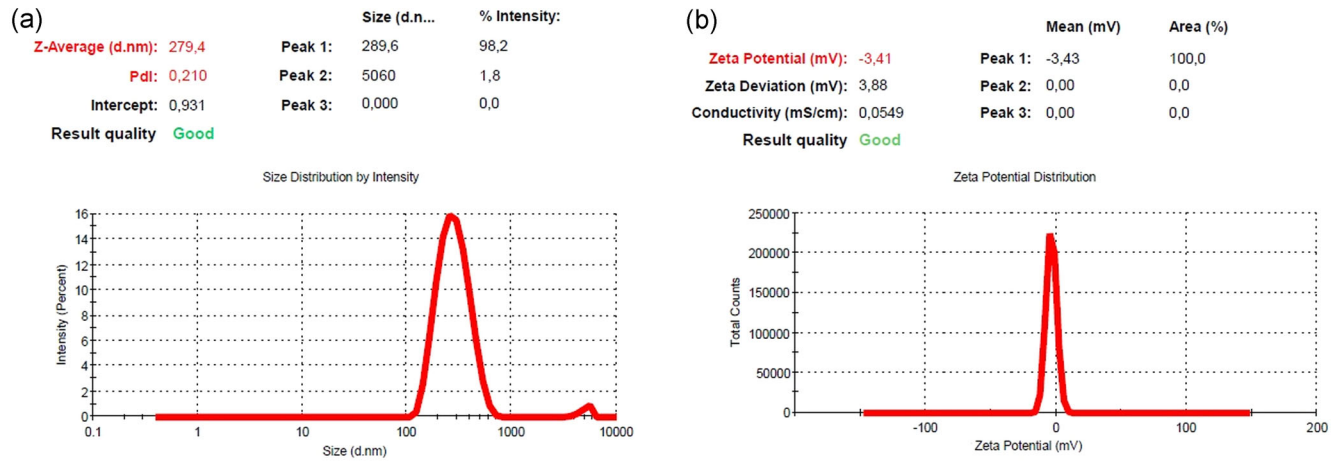

FIGURE 6 Dynamic light scattering results of ND3-loaded polycaprolactone nanoparticles: (a) average particle size and (b) ζ potential graphics

penetration and is often used to model biological activity. The rule given by Lipinski,[36] expressed as the 5's rule, defines the probability of molecules to be drug candidates: the molecular weight of ≤500, the number of hydrogen bond donor ≤5, the number of hydrogen bond acceptor ≤10, and the calculated octanol/water distribution coefficient ≤5. The ADME, drug-likeness and toxicity properties of the synthesized compounds are evaluated in Table S1 and S2.

3 | CONCLUSION

Conventional drug treatments are generally direct administrations. However, drug spreads all over the body in these types of administration and bioavailability is not in the desired amount. Also, a certain concentration of drug is required to achieve a therapeutic effect.

In this study, experimental and in silico studies were presented for drug design on cancer therapy. Our aim was to synthesize a new coumarin-based compound and the design of its nanodrug formulation for cancer treatment. It was found that the ND3 had an anticancer effect on MCF-7 and A549 cell lines, and it had no mutagenic effect. Also, it was presented that ND3-loaded PCL NPs had high drug-loading capacity, good morphological characteristics, and particle size distributions in the nano range, with a low polydispersity.

To reveal the potential use of the synthesized compound as an anticancer drug, DNA binding was indicated by experimental and in silico studies, considering that many antitumor drugs show their effects by binding to DNA. In addition, the ADME parameters, drug-likeness and toxicity properties of the synthesized compound were calculated for the first time in this study.

In conclusion, we believe that this study presents novel perspectives for the development of high drug-loading capacity in the nanomedicine field.

4 | EXPERIMENTAL

4.1 | Materials and equipment

For the synthesis of ND3, resorcinol, ethyl benzoylacetate and L-tryptophan methyl ester hydrochloride were purchased from Aldrich.

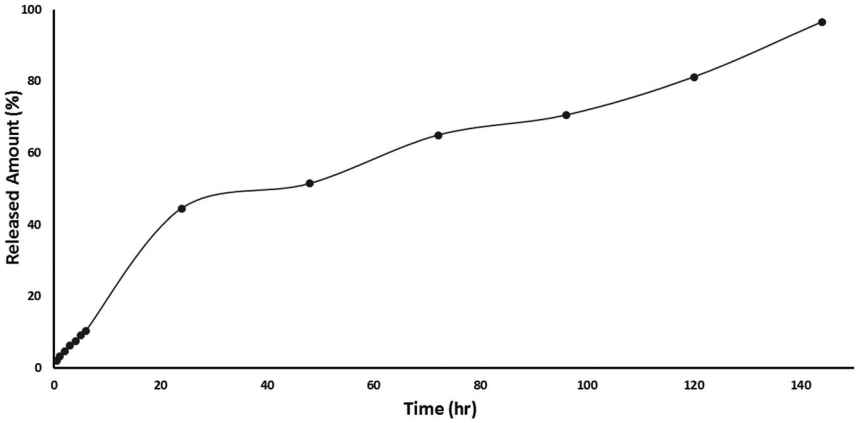

FIGURE 7 In vitro release profile of ND3 from polycaprolactone nanoparticles

TABLE 4 Mutagenicity results of ND3 on *Salmonella typhimurium* ($n = 3$ for each set of conditions)

Treatment		Concentration (μg/plate)	Number of revertant colony/plate	
			TA98 (mean ± *SD*)	TA100 (mean ± *SD*)
ND3		112	51.5 ± 10.14	122 ± 3
		108	65 ± 3	127.5 ± 2.51
		90	63.5 ± 3,6	134 ± 6.24
		78	58.5 ± 3.51	138.5 ± 22.5
		72	59.5 ± 8.18	135 ± 8.08
Positive control	NPD	10	804 ± 60.17*	–
	SA	1	–	965 ± 24.33*
Negative control (DMSO)		–	52 ± 2.08	129.5 ± 0.5
Spontaneous control		–	47.5 ± 2.51	144.5 ± 20.25

Abbreviations: DMSO, dimethyl sulfoxide; NPD, 4-nitro-*o*-phenylenediamine; SA, sodium azide; *SD*, standard deviation.
*Mutagen, the number of revertants compared with negative control is significant at the level of $p < .05$ (Tukey's test).

Reagent quality solvents were used without further purification. Column chromatography was conducted on silica gel 60 (40–63 μM; Merck). Thin-layer chromatography (TLC) was carried out on aluminum sheets precoated with silica gel $60F_{254}$ (Merck). Infrared spectra were determined on a Thermo Fisher Scientific NICOLET IS10 spectrometer. Nuclear magnetic resonance (NMR) spectra were recorded on Bruker Avance III 500-MHz spectrometer. Chemical shifts δ are reported in ppm, with tetramethylsilane as the internal standard and the solvents are $CDCl_3$. Liquid chromatography–mass spectrometry (LC–MS; quadrupole time-of-flight [QTOF]) spectra were obtained on Agilent G6530B model TOF/QTOF mass spectrometer. Optical rotations were measured with Bellingham Stanley ADP-410 polarimeter. The synthesis of 8-formyl-7-hydroxy-4-phenylcoumarin (**2**) was carried out according to the literature procedure.[37] Spectroscopic data of this compound were in accordance with its structure and literature.[38] The InChI code of ND3 is given in the Supporting Information.

Poly(vinyl alcohol) PVA (MW = 31,000–50,000, 87–89%), ethanol, CT-DNA, magnesium sulfate heptahydrate ($MgSO_4 \cdot 7H_2O$), citric acid monohydrate ($C_6H_8O_7 \cdot H_2O$), potassium phosphate, sodium dihydrogen phosphate monohydrate ($NaH_2PO_4 \cdot H_2O$), Rosewell Park Memorial Institute 1640 (RPMI-1640) medium, trypsin and fetal bovine serum (FBS) were obtained from Gibco. Dulbecco's modified Eagle's medium (DMEM) high-glucose, MTT, sodium hydroxide (NaOH), sodium chloride (NaCl), magnesium used in mutagenicity studies, chloride hexahydrate ($MgCl_2 \cdot 6H_2O$), disodium hydrogen phosphate dihydrate ($Na_2HPO_4 \cdot 2H_2O$), potassium chloride (KCl), L-histidine, D-biotin, sodium ammonium phosphate tetrahydrate ($NaHNH_4[PO_4 \cdot 4H_2O]$) and 4-nitro-*o*-phenylenediamine, which is used as a mutagen, were purchased from Sigma-Aldrich. Penicillin and streptomycin were obtained from I. E. Ulagay. Dichloromethane (DCM; >99.5%), dimethyl sulfoxide, Tris base, ethylenediaminetetraacetic acid, NaCl, hydrochloric acid and NaOH were purchased from Merck Millipore (Darmstadt, Germany). All other chemicals used in this study were of analytical grade. Ultrapure water from Millipore Milli-Q Gradient System was used to prepare the solutions. Nutrient agar, sodium azide, (SA; NaN_3) and nutrient broth were purchased from Merck Millipore. Two strains of bacteria, TA98 and

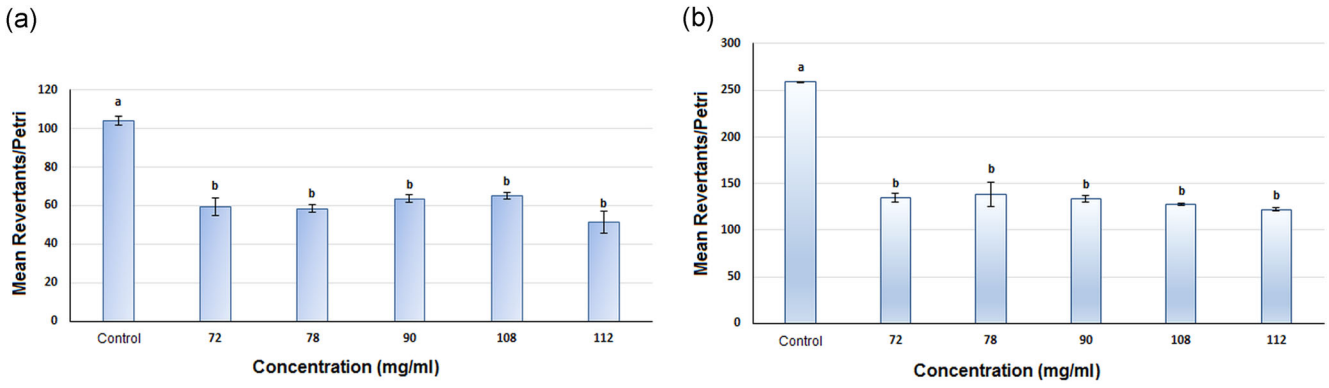

FIGURE 8 Mutagenity results of ND3 on *Salmonella typhimurium*: (a) TA98 ($p < .05$) and (b) TA100 ($p < .05$)

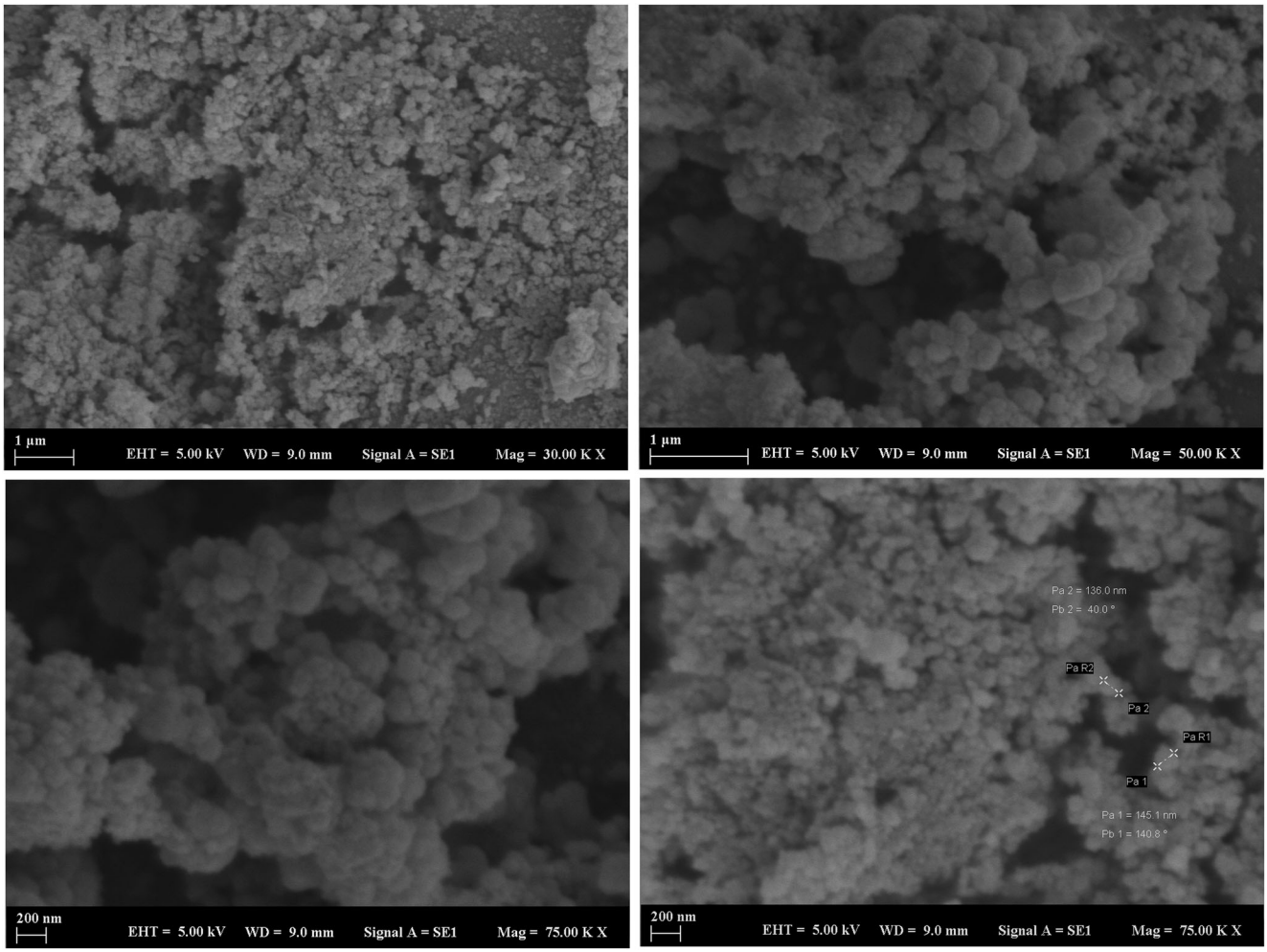

FIGURE 9 Scanning electron microscopy images of ND3-loaded polycaprolactone nanoparticles

TA100 of *Salmonella typhimurium*, were used as the test microorganisms to reveal genotoxicity and were obtained from Xenometrix. All the chemicals and solvents were of analytical grade.

4.2 | Synthesis of (*S*)-methyl 2-[(7-hydroxy-2-oxo-4-phenyl-2*H*-chromen-8-yl)methyleneamino]-3-(1*H*-indol-3-yl)propanoate (ND3)

L-Tryptophan methyl ester hydrochloride (1 mmol) in absolute ethanol (5 ml) and triethylamine (0.5 ml) suspension was stirred at room temperature for 1 hr, and then 8-formyl-7-hydroxy-4-phenylcoumarin (**2**, 1 mmol) dissolved in absolute ethanol was added. The mixture was refluxed for 2 hr. The reaction was monitored by TLC. Then alcohol was evaporated, and the crude product was purified by column chromatography on silica gel (ethyl acetate/hexane 2:3). Yellow viscous oil, yield 40%. $[\alpha]^{20}_{D} = +79.5$ (c = 1.00, $CHCl_3$). ^{1}H NMR (500 MHz, $CDCl_3$, δ): 3.34 (dd, J = 14.5, 9.0 Hz, 1H, CH_2), 3.59 (dd, J = 15.0, 5.0 Hz, 1H, CH_2), 3.78 (s, 3H, CH_3), 4.39–4.42 (m, 1H, CH), 6.10 (s, 1H, =CH), 6.74 (d, J = 9.5 Hz, 1H, ArH), 7.05 (bd, J = 3.0 Hz, 1H, ArH), 7.07–7.10 (m, 1H, ArH), 7.14–7.17 (m, 1H, ArH), 7.34 (bd, J = 7.5 Hz, 1H, ArH), 7.38–7.40 (m, 2H, ArH), 7.50–7.52 (m, 3H, ArH), 7.53–7.55 (m, 1H, ArH), 7.57–7.60 (bd, J = 8.0 Hz, 1H), 8.66 (s, 1H, CH=N) and 10.6 (bs, 1H, NH); ^{13}C NMR (125 MHz, $CDCl_3$, δ): 29.8 (CH_2), 52.6 (OCH_3), 70.2 (CH), 106.0 (C3), 109.0 (Caro), 110.1 (Caro), 111. 3 (CaroH), 111.9 (CaroH), 115.7 (CaroH), 118.4 (CaroH), 119.7 (CaroH), 122.3 (CaroH), 123.2 (CaroH), 127.0 (Caro), 128.0 (CaroH), 128.2 (CaroH), 129.0 (CaroH), 129.6 (CaroH), 131.5 (Caro), 135.4 (Caro), 136.2 (Caro), 155.2 (C4), 156.5 (Caro–OH), 161.0 (C=O) and 170.8 (C=O); FTIR (ATR): ν = 3,349 (w), 3,058 (w), 2,957, 2,925 (w), 1,730 (s), 1,626 (m), 1,582 (m), 1,477 (w), 1,378 (m) and 1,193 (m) cm^{-1}; LC–MS (ESI–QTOF): m/z $[M+H]^+$ calcd. for $C_{28}H_{23}N_2O_5$, 467.1617; found, 467.1598.

4.3 | HOMO–LUMO analysis

The HOMO–LUMO analysis and theoretical UV–Vis spectra were performed using the Gaussian 09 software program,[39] employing the time-dependent density functional theory (TD-DFT) approach

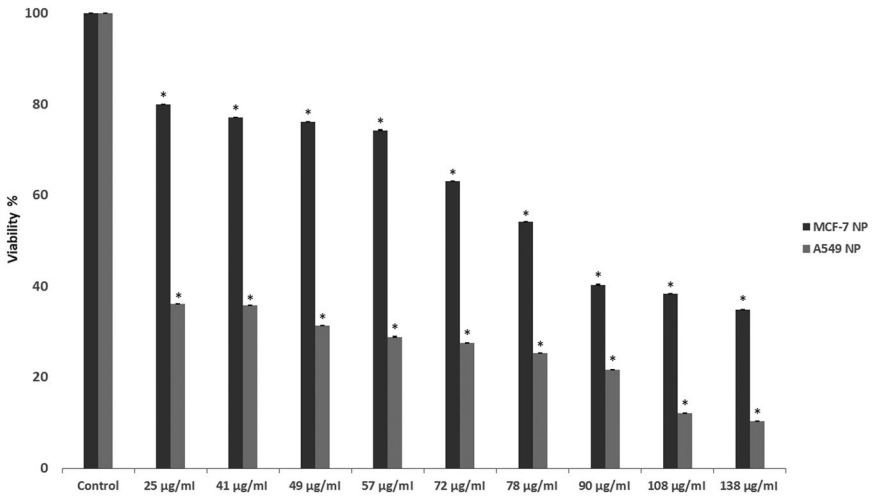

FIGURE 10 Cell viability results of ND3-loaded polycaprolactone nanoparticles against MCF-7 and A549 cell lines

based on the B3LYP/6-311++G(d,p) level to determine the bandgap (ΔE), which means the chemical stability, the ionization potential (I), the electron affinity (A), the absolute electronegativity (χ), chemical potential (μ) and the absolute hardness (η) values of the synthesized molecule were also calculated.

4.4 | DNA binding assay

The interaction between ND3 and calf thymus DNA (CT-DNA) was investigated by DNA binding assay. Briefly, Tris-HCl/NaCl buffer was used for the experiment. During the analysis, the concentration of ND3 was kept constant (36 μM), and the concentration of CT-DNA ranged from 0 to 72 μM. Changes in absorbance intensity can be calculated with percentage ratios. A formula (Equation 1) has been developed to calculate these changes.

4.5 | In vitro cell culture

Human MCF-7 cell line (ATCC® HTB-22™) was used for in vitro cytotoxicity experiments. Briefly, MCF-7 cells (10^5 cells/ml) were cultured in DMEM (Sigma-Aldrich), high-glucose medium, penicillin (100 U/ml), streptomycin (100 μg/ml) and 10% FBS (Gibco Lab) at 37°C and 5% CO_2. Cells were passaged twice a week by trypsin, and the cells were seeded at a density of 2×10^4 cells/200 μl per well in a 96-well cell culture plate for the MTT assay.

Human A549 cell line (ATCC® CCL-185™) was cultured in RPMI 1640 (Gibco Lab) medium supplemented with penicillin (100 U/ml), streptomycin (100 μg/ml) and 10% FBS (Gibco Lab), and it was incubated at 37°C with 5% CO_2. Also, 3×10^4 cells were seeded in a 96-well cell culture plate, with 200 μl/well, for the MTT assay.

4.6 | Cytotoxicity evaluation with MTT assay

Cellular viability was assessed by reduction of MTT to formazan. Briefly, MTT was dissolved in PBS and 40 μl was added to each well at a final concentration of 5 mg/ml. Cells were incubated for 4 hr at 37°C. After the incubation period, 160 μl DMSO was added to wells, followed by overnight incubation. The measurement was performed using an ELISA reader at 450–690 nm. The results are expressed relative to the control value.

4.7 | Preparation of ND3-loaded PCL NPs

ND3-loaded PCL NPs were prepared according to the double-emulsion precipitation method. Briefly, 300 mg of PCL was dissolved in 20 ml of DCM, and then 6 mg of ND3 was dissolved in 2 ml of DMSO and added to 2 ml of PCL solution. They were homogenized by applying sonication under 70 W energy for 5 min, and emulsion (w/o) was formed. Furthermore, 20 mg PVA was dissolved in 100 ml of distilled water. The (w/o) emulsion was pulled with a syringe and then added dropwise into the PVA solution with continuous stirring. Then, the mixture was homogenized by applying sonication under 70 W energy for 5 min, and double emulsion (w/o/w) was formed. The mixture was left overnight with continuous stirring. The obtained

TABLE 5a The binding affinity, close interactions, and hydrogen bonding interaction of ND3 bound by B-DNA dodecamer

ND3		
Affinity (kcal/mol)	**Close interactions**	**Hydrogen bonding (Å)**
−8.8	DG10, DG12, DG14, DG16, DA17, DA18, DC9, DC11, DT19	DG10, DG16

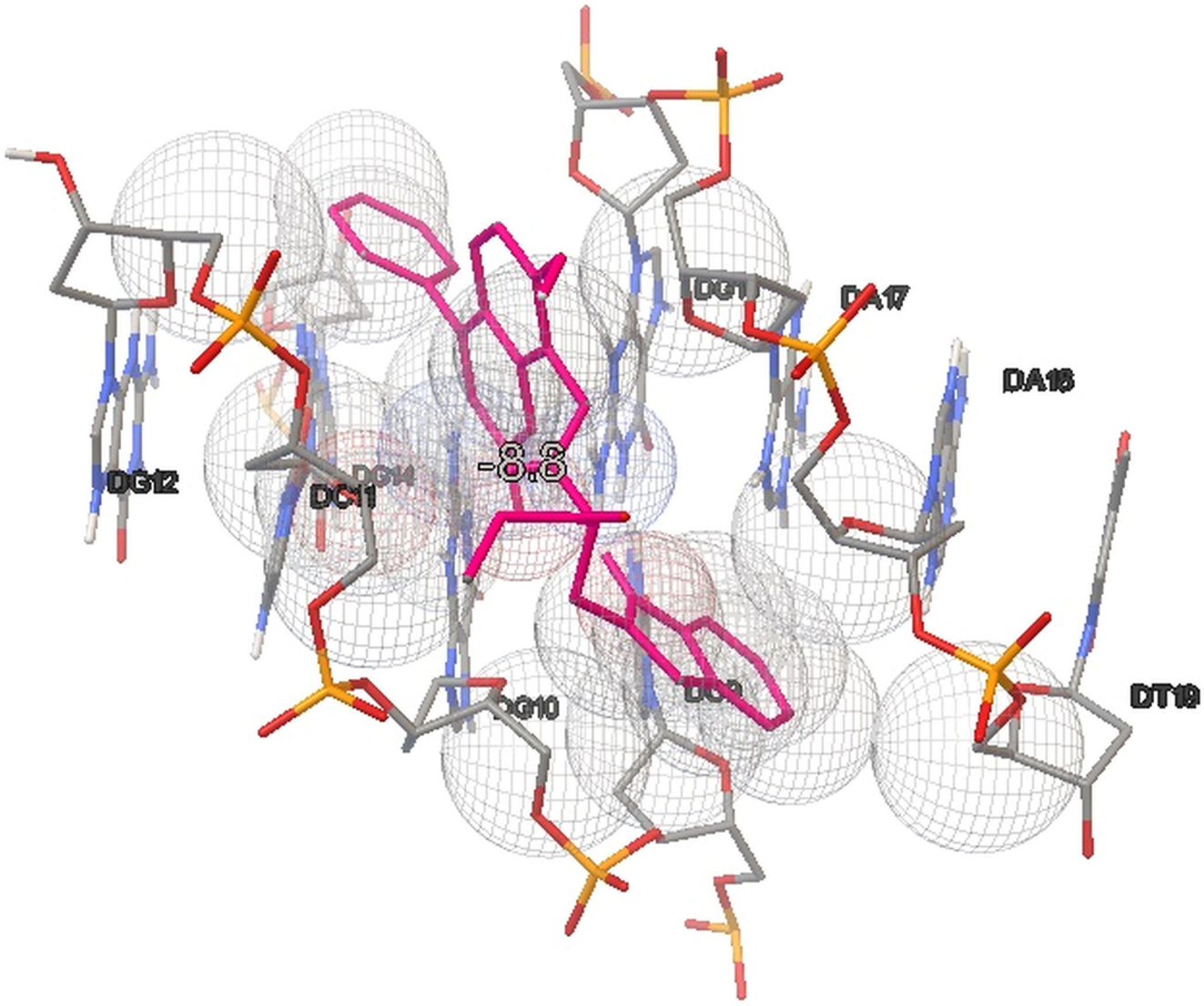

FIGURE 11 The best-docked pose of ND3 with the B-DNA

ND3-loaded PCL NPs were centrifuged at 10,000 rpm for 45 min and washed five times to remove any residual organic solvent. To prepare blank PCL NPs, the remaining steps were performed for equal amounts without ND3, as described above. Finally, blank and ND3-loaded PCL NPs were freeze-dried for further characterization and others analysis.

4.8 | Preparation of the standard curve

In total, eight different concentrations of ND3 (0.195313, 0.390625, 0.78125, 1.5625, 3.125, 6.25, 12.5 and 25 μg/ml) were prepared by serial dilution. The UV absorbance value of each concentration was determined at 231.5 nm by UV–Vis spectrometer. Then the standard curve was obtained (Figure 4), and the curve equation was used to determine the encapsulation efficiency and loading capacity.

4.9 | Determination of encapsulation efficiency and loading capacity

The concentration of free ND3 in the supernatant was determined by the equation of ND3 standard curve (Figure 4), and the encapsulation efficiency and loading capacity were calculated using the following equations:

$$\text{Encapsulation efficiency}(\%) = \frac{\text{Total ND3 amount} - \text{Free ND3 amount}}{\text{Total ND3 amount}} \times 100, \quad (3)$$

$$\text{Loading capacity}(\%) = \frac{\text{Encapsulated ND3}}{\text{Total NPs weight}} \times 100. \quad (4)$$

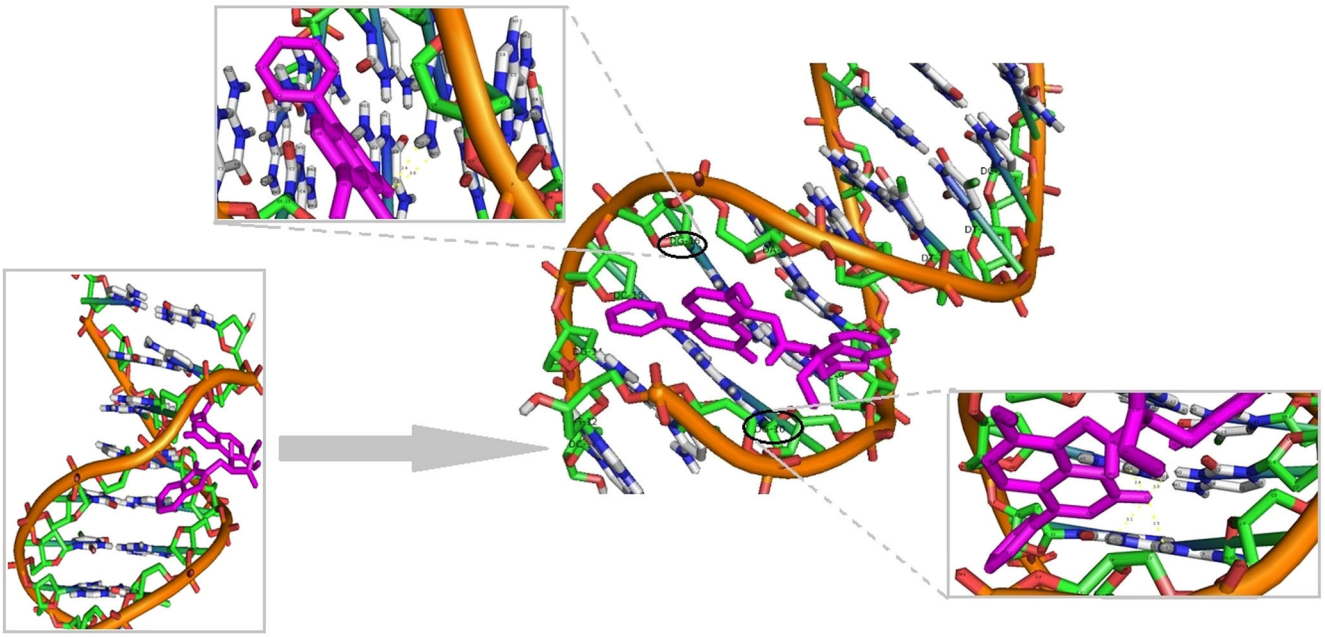

FIGURE 12 The hydrogen bonding interactions between ND3 and the B-DNA

TABLE 5b The atoms of close interactions between ND3 and B-DNA dodecamer

DNA chain	Residues of DNA	Atom number of residues of DNA	Atom of conformer-1	Interaction (Å)
A	DG10	H3	O1 (ND3)	2.5
A	DG10	H22	O1 (ND3)	3.1
B	DG16	H22	O1 (ND3)	2.4
B	DG16	H21	O1 (ND3)	3.0

TABLE 6 The root mean squared deviation (RMSD) values of ND3 bounded by B-DNA dodecamer

Mode	Affinity (kcal/mol)	Distribution from RMSD l.b.	Best mode RMSD l.b.
1	−8.8	0.000	0.000
2	−8.6	1.205	1.668
3	−8.6	1.911	3.443
4	−8.5	2.245	3.900
5	−8.3	2.601	9.064
6	−8.2	2.445	5.051
7	−8.2	2.335	9.150
8	−8.0	12.339	13.747
9	−7.8	3.307	9.719

4.10 | DLS analysis

The physicochemical properties of NPs were analyzed by using the DLS technique. The average particle size, polydispersity index and ζ potential values of NPs were determined by Zetasizer Nano ZS (Malvern Instruments Ltd., Malvern, UK). The 4-mW He–Ne laser was used at a wavelength of 633 nm with a detection angle of 90°. All measurements were made at a temperature of 25°C, and each sample was prepared with a PBS solution before filtering with a 0.45-μm regenerated cellulose membrane (Sartorius, Germany). The particle size, ζ potential and PdI were reported as the mean of at least 10 measurements.

4.11 | Scanning electron microscopy (SEM) analysis

The morphology of the ND3-loaded PCL NPs was revealed using SEM (Zeiss Supra 50 V). Briefly, the samples were diluted with ethanol and placed directly in an ultrasound bath for 15 min. Then, the samples were prepared by dropping 40 μl of ND3-loaded PCL NPs on the SEM stubs, which were covered with aluminum foil, and they were dried for 1 day at room temperature. The SEM images were obtained at ×100.00 k magnification, 5.00 kV electron high tension and 9.0 mm working distance with an in-lens detector.

4.12 | In vitro release study

ND3-loaded PCL NPs were dispersed in 2 ml distilled water and placed in a dialysis capsule to determine the in vitro release profile of

ND3. Phosphate buffer (PBS) at pH 7.4 was used as the release medium. In vitro release study was performed at time intervals 0, 0.5, 1, 2, 3, 4, 5, 6, 7, 8, 24, 48, 72, 96, 120 and 144 hr. Incubation of samples was achieved in a shaking water bath at 37°C under gentle agitation. At each time intervals, a 1-ml sample was taken from the release medium, and fresh release medium of the same volume was added instead. The samples were analyzed by UV–Vis spectrometer, and the amount of ND3 released from the PCL NPs, depending on time, was obtained by using the following equation:

$$\text{Release}(\%) = \frac{\text{Released ND3}}{\text{Total ND3}} \times 100. \quad (5)$$

4.13 | Ames/*Salmonella* mutagenicity assay

The TA98 and TA100 strains of *S. typhimurium* were used to determine the frameshift and basepair change mutation of the ND3. Experiments were performed as described by Maron and Ames.[40,41] Briefly, the concentrations of ND3 used in the experiment were determined depending on the in vitro release profile of ND3 (five different concentrations: 72, 78, 90, 108 and 112 µg). To ensure the reliability of the experiment, first, it was checked whether the test strains had original mutations. Therefore, histidine requirement, presence of R factor, rfa mutation and uvrB mutation of the test strains were controlled before starting the study. Before performing the experiment, a single fresh colony of standard strains of *S. typhimurium* TA98 and TA100 was inoculated in nutrient broth and incubated for 10–12 hr at 37°C in an incubator. Each strain of *S. typhimurium* was grown separately in Erlenmeyer flasks. Autoclaved distilled water was used as a negative control, and sodium azide (1 µg/plaque) and 4-nitro-*o*-phenylenediamine (10 µg/plaque) were used as positive controls for TA98 and TA100 without S9 metabolic activation. 2-Aminofluorene (5 µg/plaque) was prepared for TA98 and TA100 metabolic activation. For mutagenity study, 222 µL of histidine-biotin solution, 500 µL of sodium-phosphate buffer, 100 µL of sample and controls, and 100 µL of bacterial culture were added to 2 ml top agar kept at 43°C and top agar was poured into minimal glucose agar (MGA). Then, they were mixed gently and poured into MGA plaque. These plaques were incubated at 37°C for 48 hr. Spontaneous revertant colonies (His + revertants) were counted at the end of the incubation.

4.14 | Molecular docking analysis

The aim of molecular docking is to give a prediction of the small molecule and receptor such as DNA, RNA, protein, enzyme and so forth. The structure of a B-DNA dodecamer (PDB: 1BNA)[26] with 1.9 Angstrom resolution was used as a target receptor for molecular docking analysis. All water molecules and ions were deleted, and the polar hydrogens were added to the receptor before the docking calculation. The molecular structure of the synthesized compound was prepared and optimized with DFT/B3LYP 6-311++G(d,p) basis set using Gaussian software.[39] For docking analysis, all.pdb files were converted to.pdbqt file format via docking protocol. The grid boxes were adjusted to $X = 40$ Å, $Y = 40$ Å and $Z = 40$ Å with 0.375-nm grid spacing. AutoDockVina 1.1.2 program[42] was implemented for docking analysis that was used to define the most favorable binding affinities and RMSD values for the synthesized compound. The close interactions, binding affinities, and RMSD were calculated as a result of the study. Energy-scoring function is used to determine the best ligand–DNA pose. PyMol 2.2.3[43] and AutoDockTools1.5.6[44] programs were used to observe close interactions and hydrogen bonding interactions.

4.15 | Statistical analysis

For the statistical analysis of Ames/*Salmonella* mutagenicity assay, the data obtained from the experimental and control groups were compared using the SPSS program (version 24.0; SPSS Science, Chicago, IL). Significant differences are indicated by a–b ($p < .05$, Tukey's honestly significant difference test) among doses in the same dose column. The $p < .05$ was accepted as significant in all statistical evaluations.

For statistical analysis of the cytotoxicity experiments, one-way analysis of variance test were used to analyze experimental groups followed by post-hoc Tukey multiple comparisons. A $p < .05$ was considered statistically significant (Prism Version 7.0; GraphPad Software, Inc.).

ACKNOWLEDGMENTS

The authors would like to thank TUBITAK for its support through the Yildiz Technical University Scientific Research Foundation (project number FBA-2017-3168). In this study, the infrastructure of Applied Nanotechnology and Antibody Production Laboratory established with TUBITAK support (project numbers: 115S132 and 117S097) was used.

CONFLICTS OF INTERESTS

The authors declare that there are no conflicts of interests.

ORCID

Cigdem Yolacan http://orcid.org/0000-0003-4221-3592

REFERENCES

[1] K.-G. Weng, Y.-L. Yuan, *Braz. J. Med. Biol. Res.* **2017**, *50*, e6455. https://doi.org/10.1590/1414-431X20176455
[2] M. Kaur, S. Kohli, S. Sandhu, Y. Bansal, G. Bansal, *Anti-Cancer Agents Med. Chem.* **2015**, *15*, 1032. https://doi.org/10.2174/1871520615666150101125503
[3] A. Sabt, O. M. Abdelhafez, R. S. El-Haggar, H. M. F. Madkour, W. M. Eldehna, E. El-D. A. M. El-Khrisy, M. A. Abdel-Rahman, L. A. Rashed, *J. Enzyme Inhib. Med. Chem.* **2018**, *33*, 1095. https://doi.org/10.1080/14756366.2018.1477137
[4] J. Dandriyal, R. Singla, M. Kumar, V. Jaitak, *Eur. J. Med. Chem.* **2016**, *119*, 141. https://doi.org/10.1016/j.ejmech.2016.03.087
[5] O. C. Farokhzad, R. Langer, *ACS Nano* **2009**, *3*, 16. https://doi.org/10.1021/nn900002m
[6] R. A. Petros, J. M. de Simone, *Nat. Rev. Drug Discov.* **2010**, *9*. https://doi.org/10.1038/nrd2591615
[7] A. Aghebati-Maleki, S. Dolati, M. Ahmadi, A. Baghbanzhadeh, M. Asadi, A. Fotouhi, M. Yousefi, L. Aghebati-Maleki, *J. Cell. Physiol.* **2020**, *235*, 1962. https://doi.org/10.1002/jcp.29126

[8] S. Cesmeli, C. B. Avci, *J. Drug Targets* **2019**, *27*, 762. https://doi.org/10.1080/1061186X.2018.1527338
[9] L. P. Krishnamoorthy, R. K. Moorthy, D. Umapathy, M. K. Kannan, N. Ganesan, A. J. V. Arockiam, *Clin. Oncol.* **2017**, *2*, 1325.
[10] S. Naahidi, M. Jafari, F. Edalat, K. Raymond, A. Khademhosseini, P. Chen, *J. Contr. Rel.* **2013**, *166*, 182. https://doi.org/10.1016/j.jconrel.2012.12.013
[11] M. A. Woodruff, D. W. Hutmacher, *Prog. Polym. Sci.* **2010**, *35*, 1217.
[12] S. Zhang, H. Uludag, *Pharm. Res.* **2009**, *26*, 1561. https://doi.org/10.1007/s11095-009-9897-z
[13] L. Zhang, Y.-C. Yao, M.-Y. Gao, R.-X. Rong, K.-R. Wang, X.-L. Li, H. Chen, *Chin. Chem. Lett.* **2016**, *27*, 1708. https://doi.org/10.1016/j.cclet.2016.05.027
[14] A. Bisi, C. Cappadone, A. Rampa, G. Farruggia, A. Sargenti, F. Belluti, R. M. C. Di Martino, E. Malucelli, A. Meluzzi, S. Lotti, S. Gobbi, *Eur. J. Med. Chem.* **2017**, *127*, 577. https://doi.org/10.1016/j.ejmech.2017.01.020
[15] D. Cao, Y. Liu, W. Yan, C. Wang, P. Bai, T. Wang, M. Tang, X. Wang, Z. Yang, B. Ma, L. Ma, L. Lei, F. Wang, B. Xu, Y. Zhou, T. Yang, L. Chen, *J. Med. Chem.* **2016**, *59*, 5721. https://doi.org/10.1021/acs.jmedchem.6b00158
[16] M. A. I. Salem, M. I. Marzouk, A. M. El-Kazak, *Molecules* **2016**, *21*, 249. https://doi.org/10.3390/molecules21020249
[17] H. A. Garro, G. F. Reta, O. J. Donadel, C. R. Pungitore, *Nat. Prod. Commun.* **2016**, *11*, 1289. https://doi.org/10.1177/1934578X1601100926
[18] N. Jalilzadeh, N. Samadi, R. Salehi, G. Dehghan, M. Iranshahi, M. R. Dadpour, H. Hamishehkar, *Sci. Rep.* **2020**, *10*, 1606. https://doi.org/10.1038/s41598-020-58527-0
[19] J. Trykowska Konc, E. Hejchman, H. Kruszewska, I. Wolska, D. Maciejewska, *Eur. J. Med. Chem.* **2011**, *46*, 2252. https://doi.org/10.1016/j.ejmech.2011.03.006
[20] E. A. Fayed, R. Sabour, M. F. Harras, A. B. M. Mehany, *Med. Chem. Res.* **2019**, *28*, 1284. https://doi.org/10.1007/s00044-019-02373-x
[21] S. A. Morsy, A. A. Farahat, M. N. A. Nasr, A. S. Tantawy, *Saudi Pharm. J.* **2017**, *25*, 873. https://doi.org/10.1016/j.cclet.2016.05.027
[22] A. Y. Hassan, M. T. Sarg, M. A. El Deeb, A. H. Bayoumi, S. I. El Rabeb, *J. Het. Chem.* **2018**, *55*, 1426. https://doi.org/10.1002/jhet.3179
[23] K. M. Amin, A. M. Taha, R. F. George, N. M. Mohamed, F. F. Elsenduny, *Arch. Pharm. Chem. Life Sci.* **2018**, *351*, e1700199. https://doi.org/10.1002/ardp.201700199
[24] K. Fukui, *Science* **1982**, *218*, 747. https://doi.org/10.1126/science.218.4574.747
[25] A. Nataraj, V. Balachandran, T. Karthick, *J. Mol. Struct.* **2013**, *1031*, 221. https://doi.org/10.1016/j.molstruc.2012.09.047
[26] H. R. Drew, R. M. Wing, T. Takano, C. Broka, S. Tanaka, K. Itakura, R. E. Dickerson, *Prod. Natl. Acad. Sci. USA* **1981**, *78*, 2179. https://doi.org/10.1073/pnas.78.4.2179
[27] S. U. Rehman, T. Sarwar, M. A. Husain, H. M. Ishqi, M. Tabish, *Arch. Biochem. Biophys.* **2015**, *576*, 49. https://doi.org/10.1016/j.abb.2015.03.024
[28] M. Sirajuddin, S. Ali, A. Badshah, *J. Photochem. Photobiol. B* **2013**, *124*. https://doi.org/10.1016/j.jphotobiol.2013.03.0131
[29] Y. Budama-Kilinc, *Sci. Adv. Mater.* **2019**, *11*, 738. https://doi.org/10.1166/sam.2019.3541
[30] Y. Song, D. Zhong, J. Luo, H. Tan, S. Chen, P. Li, L. Wang, T. Wang, *Luminescence* **2014**, *29*, 1141. https://doi.org/10.1002/bio.2674
[31] M. Shebl, *Spectrochim. Acta A* **2014**, *117*, 127. https://doi.org/10.1016/j.saa.2013.07.107
[32] G. Bischoff, S. Hoffmann, *Curr. Med. Chem.* **2002**, *9*, 321. https://doi.org/10.2174/0929867023371085
[33] S. Shen, Y. Wu, Y. Liu, D. Wu, *Int. J. Nanomed.* **2017**, *12*, 4085. https://doi.org/10.2147/IJN.S132780
[34] K. Mortelmans, E. Zeiger, *Mutat. Res.* **2000**, *455*, 29. https://doi.org/10.1016/s0027-5107(00)00064-6
[35] P. Ertl, B. Rohde, P. Selzer, *J. Med. Chem.* **2000**, *43*, 3714. https://doi.org/10.1021/jm000942e
[36] C. A. Lipinski, F. Lombardo, B. W. Dominy, P. J. Feeney, *Adv. Drug Deliv. Rev.* **1997**, *23*. https://doi.org/10.1016/s0169-409x(00)00129-03
[37] A. Kulkarni, S. A. Patil, P. S. Badami, *Eur. J. Med. Chem.* **2009**, *44*, 2904. https://doi.org/10.1016/j.ejmech.2008.12.012
[38] V. S. Moskvina, V. P. Khilya, *Chem. Nat. Compd.* **2008**, *44*, 16. https://doi.org/10.1007/s10600-008-0006-z
[39] M. J. E. A. Frisch, G. W. Trucks, H. B. Schlegel, G. E. Scuseria, M. A. Robb, J. R. Cheeseman, H. Nakatsuji, *Gaussian 09*, *Revision A. 02*, 200, Gaussian. Inc., Wallingford, CT **2009**, p. 28.
[40] U. Vijay, S. Gupta, P. Mathur, P. Suravajhala, P. Bhatnagar, *Bio-protocol* **2018**, *8*, e2763. https://doi.org/10.21769/BioProtoc.2763
[41] L. D. Kier, *Regul. Toxicol. Pharm.* **1985**, *5*, 59. https://doi.org/10.1016/0273-2300(85)90020-0
[42] O. Trott, A. J. Olson, *J. Comput. Chem.* **2010**, *31*, 455. https://doi.org/10.1002/jcc.21334
[43] Schrödinger L.L.C., *The PyMOL Molecular Graphics System*, *Version 2.0*, Schrödinger LLC, New York, NY **2017**.
[44] R. Huey, G. M. Morris, S. Forli, *Using AutoDock 4 and AutoDock Vina with AutoDockTools: A Tutorial*, The Scripps Research Institute Molecular Graphics Laboratory, California **2012**.

SUPPORTING INFORMATION

Additional supporting information may be found online in the Supporting Information section.

How to cite this article: Budama-Kilinc Y, Kecel-Gunduz S, Ozdemir B, et al. New nanodrug design for cancer therapy: Its synthesis, formulation, in vitro and in silico evaluations. *Arch Pharm*. 2020;e2000137. https://doi.org/10.1002/ardp.202000137